EARTH SURFACE PROCESSES AND LANDFORMS
Earth Surf. Process. Landforms **37**, 546–561 (2012)
Published in 2012 by John Wiley and Sons, Ltd.
Published online 31 January 2012 in Wiley Online Library
(wileyonlinelibrary.com) DOI: 10.1002/esp.3192

Progressive failure of sheeted rock slopes: the 2009–2010 Rhombus Wall rock falls in Yosemite Valley, California, USA

Greg M. Stock,[1]* Stephen J. Martel,[2] Brian D. Collins[3] and Edwin L. Harp[4]
[1] National Park Service, Yosemite National Park, El Portal, California, USA 95318
[2] Department of Geology and Geophysics, University of Hawaii, Honolulu, Hawaii, USA 96822
[3] U.S. Geological Survey, Landslide Hazard Program, Menlo Park, California, USA 94025
[4] U.S. Geological Survey, Landslide Hazard Program, Golden, Colorado, USA 80225

Received 1 June 2011; Revised 3 December 2011; Accepted 5 December 2011

*Correspondence to: G. M. Stock, National Park Service, Yosemite National Park, Resources Management and Science, 5083 Foresta Road, PO Box 700, El Portal, California 95318, USA. E-mail: greg_stock@nps.gov

ESPL
Earth Surface Processes and Landforms

ABSTRACT: Progressive rock-fall failures in natural rock slopes are common in many environments, but often elude detailed quantitative documentation and analysis. Here we present high-resolution photography, video, and laser scanning data that document spatial and temporal patterns of a 15-month-long sequence of at least 14 rock falls from the Rhombus Wall, a sheeted granitic cliff in Yosemite Valley, California. The rock-fall sequence began on 26 August 2009 with a small failure at the tip of an overhanging rock slab. Several hours later, a series of five rock falls totaling 736 m^3 progressed upward along a sheeting joint behind the overhanging slab. Over the next 3 weeks, audible cracking occurred on the Rhombus Wall, suggesting crack propagation, while visual monitoring revealed opening of a sheeting joint adjacent to the previous failure surface. On 14 September 2009 a 110 m^3 slab detached along this sheeting joint. Additional rock falls between 30 August and 20 November 2010, totaling 187 m^3, radiated outward from the initial failure area along cliff (sub)parallel sheeting joints. We suggest that these progressive failures might have been related to stress redistributions accompanying propagation of sheeting joints behind the cliff face. Mechanical analyses indicate that tensile stresses should occur perpendicular to the cliff face and open sheeting joints, and that sheeting joints should propagate parallel to a cliff face from areas of stress concentrations. The analyses also account for how sheeting joints can propagate to lengths many times greater than their depths behind cliff faces. We posit that as a region of failure spreads across a cliff face, stress concentrations along its margin will spread with it, promoting further crack propagation and rock falls. Published in 2012. This article is a US Government work and is in the public domain in the USA.

KEYWORDS: rock fall; progressive failure; sheeting joints; crack propagation; Yosemite National Park

Introduction

Progressive failures are common on natural rock slopes and within excavated tunnels (Eberhardt *et al.*, 2004; Kemeny, 2005; Rosser *et al.*, 2007; Jaboyedoff *et al.*, 2009). The term 'progressive' generally refers to time-dependent structural changes that act to reduce slope stability and ultimately lead to slope failure (Terzaghi, 1950). Here, we use the term to describe failure progressions in space as well as time; e.g. subsequent failures that occur along the perimeter of a previous failure.

Progressive slope failures have long been recognized in the field of soil mechanics, wherein failure initiates at a point along a potential sliding surface and propagates outwards from it, with propagation driven primarily by redistribution of shear stresses (Bishop, 1967; Bjerrum, 1967). A similar phenomenon involving progressive rupture along faults is referred to as 'stress triggering' in the field of seismotectonics (Stein *et al.*, 1997). In hard rock slopes, progressive failure typically involves the time-dependent propagation of discontinuities in the rock, e.g. cracks, joints, faults, and fissures (Terzaghi, 1962). Time-dependent failures along discontinuities can occur for several reasons, including weathering of the failure surface, viscous deformation of fracture-filling material, and subcritical crack growth (Atkinson, 1984; Kemeny, 2005; Petley *et al.*, 2005). Time-dependent failure along discontinuities can also result from fracture propagation through intact rock 'bridges' that separate pre-existing discontinuities (Einstein *et al.*, 1983; Goodman and Kieffer, 2000; Eberhardt *et al.*, 2004; Kemeny, 2005; Kim and Kemeny, 2009). Here we consider a related mechanism, that of propagation of sheeting joints (also known as 'exfoliation' joints) driven both by areal tensile stresses perpendicular to a sheeted cliff face and by localized stress concentrations arising from geometrical changes to the cliff face resulting from previous rock falls.

Sheeting joints are opening mode rock fractures that form (sub)parallel to topographic surfaces. They are gently curved, occur most commonly where the topography is convex, and

can extend in plane at least 200 m (Gilbert, 1904; Matthes, 1930; Jahns, 1943; Bahat *et al.*, 1999). Sheeting joints occur from within a meter of the modern surface to depths in excess of 100 m and typically develop independent of the grain scale rock structure (Jahns, 1943). They are most widespread in granitic rocks and gneisses, but have also been observed in mafic intrusive rocks, sandstones, marbles, and tuffs (Holzhausen, 1989). High compressive stresses parallel to the surface consistently have been either inferred from field observations (buckling of rock slabs bounded by sheeting joints) or measured where sheeting joints are prominent (Martel, 2006, 2011). Sheeting joints have been observed to form in quarries (Jahns, 1943; Holzhausen, 1989), and several lines of evidence suggest that many sheeting joints in Yosemite are geologically young, with some nucleating, opening, and propagating historically (Martel, 2006, 2011, and references therein). We suggest that the geometry of sheeting joints, and the mechanical factors controlling how sheeting joints grow, are important considerations when analyzing progressive rock slope failures, and present as an example a well-documented sequence of rock falls in Yosemite Valley.

Although progressive slope failures are relatively common, quantitative field studies remain scarce, particularly for natural rock slopes. This is probably due to the difficulty in anticipating these events and ensuring that quantitative reference points are in place and accurately located prior to failure. Recent studies of progressive slope failures have utilized terrestrial laser scanning (lidar), which provides high-resolution topographic data (Rosser *et al.*, 2007; Jaboyedoff *et al.*, 2009; Kemeny and Kim, 2009). Laser scanning is a valuable tool for quantitative, high-resolution investigation of slope failures, particularly when repeat scans bracket failure events (Collins and Sitar, 2005, 2008; Rosser *et al.*, 2005; Abellán *et al.*, 2006; Oppikofer *et al.*, 2008; Rabatel *et al.*, 2008; Stock *et al.*, 2011).

Here we describe a 1.2-year-long sequence of 15 rock falls from the Rhombus Wall, a sheeted granitic cliff in eastern Yosemite Valley, California, USA (Figure 1), which occurred sporadically between 26 August 2009 and 20 November 2010. We documented the progressive nature of these events with a combination of visual monitoring, repeat high-resolution digital photography, video, and airborne and terrestrial laser scanning data collected between rock-fall events. The sequence of rock falls in time, coupled with their distribution on the cliff, provide insight into the nature of progressive failure of sheeted rock slopes, and the stress redistribution and associated crack propagation that might accompany these failures. We also explore the mechanics of sheeting joint propagation to develop a better understanding of the stress conditions surrounding the Rhombus Wall rock falls.

Progressive Rock Falls in Yosemite Valley

With its nearly 1-km-tall glacially steepened cliffs and fractured granite walls, rock falls are common in Yosemite National Park. From 1857 to 2010, 836 mass wasting events were documented in the park, including rock falls, rock slides, debris flows, etc. (Wieczorek and Snyder, 2004, and additional unpublished observations). Of these documented events, 72% were rock falls and rock slides from the cliffs of Yosemite Valley, a 14 km-long glacially carved valley in Cretaceous granitic rocks of the Sierra Nevada mountain range that was deglaciated approximately 15–17 ka (Matthes, 1930; Huber, 1987).

A network of regional discontinuities (fractures and dikes) forms the dominant geologic structure of Yosemite Valley and the surrounding area (Matthes, 1930; Huber, 1987; Matasci *et al.*, 2011). Although these regional discontinuities play an important role in controlling the local topography, the most common fractures exposed in Yosemite are sheeting joints formed (sub)parallel to modern topographic surfaces (Matthes, 1930; Huber, 1987; Bahat *et al.*, 1999; Martel, 2006, 2011). Rock falls in Yosemite Valley commonly detach along sheeting joints (Wieczorek and Snyder, 1999, 2004; Stock *et al.*, 2011). Sheeting joints are ubiquitous at the site of the Rhombus Wall rock falls (Figure 1), although other regional fractures and dikes are also present there.

A review of historical rock falls (Wieczorek and Snyder, 2004, and additional unpublished observations) yields numerous examples of progressive rock falls in Yosemite Valley, in which a series of two or more rock falls occurred from adjacent locations on a cliff face (i.e. the failure surface of each subsequent rock fall shared a perimeter with a previous rock fall) within a 1-year time period. Most of these rock falls originated along sheeting joints; recent examples include the 1998–1999 Glacier Point rock falls above Curry Village (Wieczorek and Snyder, 1999), rock falls from Half Dome in July of 2006, the October 2008 Glacier Point rock falls above the Ledge Trail (Stock *et al.*, 2011), and rock falls from El Capitan in October of 2010. In addition, several historical rock falls in Yosemite Valley have been associated either with observed crack propagation or with cracking sounds – presumably reflecting crack propagation – prior to failure. Following the third rock fall from Glacier Point between November 1998 and June 1999, Wieczorek and Snyder (1999) observed crack propagation occurring in an adjacent sheet of rock, probably due to stress redistribution in the cliff after the 13 June 1999 rock fall. Audible cracking preceded the 16 November 1980 rock fall from above the Yosemite Falls Trail, which caused three fatalities and at least 11 injuries (Wieczorek and Snyder, 2004), and also the October 2008 rock falls from Glacier Point, which damaged 25 visitor cabins in Curry Village and caused minor injuries (Stock *et al.*, 2011).

Given the possibility of remotely monitoring fracture propagation, either through direct observation of cliffs (Wieczorek and Snyder, 1999; Ishikawa *et al.*, 2004) or through remote methods such as acoustic or seismic monitoring (Zimmer *et al.*, 2012), quantitative documentation of fracture propagations and time-dependent rock falls can be an important step towards predicting future rock falls (Rosser *et al.*, 2007). The sequence of rock falls from the Rhombus Wall, documented in high resolution, provides insight into processes that drive progressive rock falls from natural rock slopes.

Remote Sensing Data Acquisition and Analysis

High-resolution photography and video

High-resolution digital photographs of the rock-fall source area and adjacent cliff before, during, and after each major rock fall event aided our quantitative analysis of the Rhombus Wall rock falls. We obtained pre-rock fall images from gigapixel panoramic photographs of Yosemite Valley (Figure 1 (B)), which can be zoomed-in on to reveal the rock-fall source area prior to failure (Figure 1(C)). Stock *et al.* (2011) provide details of the acquisition of these photos, which are available for viewing at http://www.xrez.com/case-studies/national-parks/yosemite-extreme-panoramic-imaging-project/. Because most of the Rhombus Wall rock falls occurred during daylight hours, and often in quick succession, park visitors and employees captured numerous high-resolution

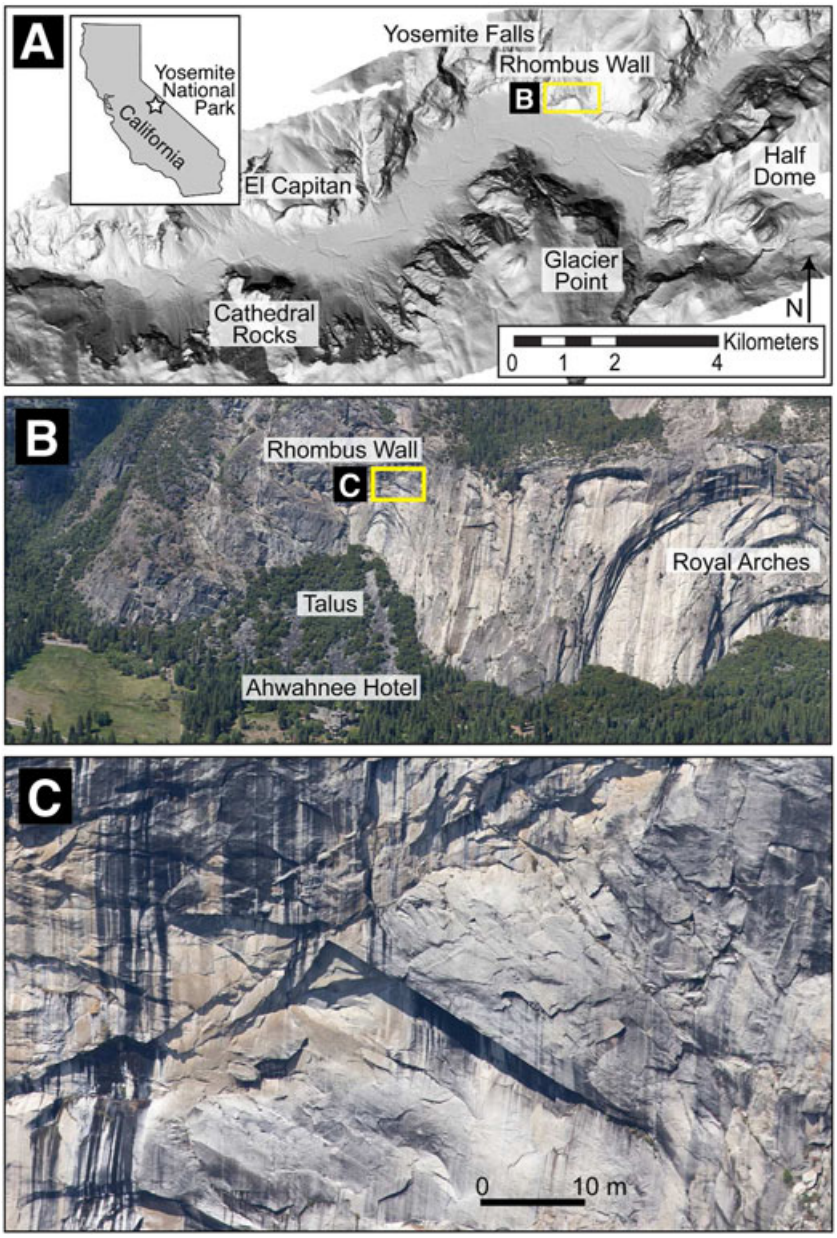

Figure 1. Rhombus Wall rock-fall source area. (A) Shaded relief map of Yosemite Valley, derived from a 1 m resolution lidar-based digital elevation model, showing location of Rhombus Wall (yellow box). Inset shows location of Yosemite National Park in eastern California. (B) Photograph of the Rhombus Wall, view to the north, showing the 2009–2010 rock-fall source area (yellow box). (C) Zoomed-in view of the source area prior to the 2009–2010 rock falls; the failures occurred above and left of the overhanging shadowed roof that extends from lower right to upper left in the center of the photograph (compare with Figure 5). This figure is available in colour online at wileyonlinelibrary.com/journal/espl

digital photographs and video of the rock falls as they occurred (Figure 2). After each rock fall event, we repeated the digital photography to produce high-resolution before-and-after photos.

Airborne laser scanning

In September of 2006, prior to the first Rhombus Wall rock fall that we studied, airborne laser scanning (lidar) data were collected for Yosemite Valley and vicinity, an area of ~43 km^2. This area includes the Rhombus Wall located north of the Ahwahnee Hotel (Figure 1). Airborne lidar data were collected with an Optech 1233 ALTM scanner mounted in a turbocharged twin engine Cessna 337. Flying heights above ground level varied from less than 100 m to more than 2 km, with an average height of 1050 m. The average resultant point spacing on the cliff typically ranged from 0.75 to 2.25 m.

Terrestrial laser scanning

Following the initial Rhombus Wall rock falls of August 2009, and after each subsequent major rock fall, we collected terrestrial lidar data for the rock-fall source area and vicinity. We employed a Riegl Z420i laser scanner fixed to a tilt-mount to provide a more perpendicular viewing angle of the upper cliff. A Nikon D200 digital SLR camera, mounted and calibrated to the laser, was used to color the point cloud for visualization purposes. In total, we collected five terrestrial lidar data sets (acquired on 5 September 2009, 3 November 2009, 7 July 2010, 12 October 2010, and 14 December 2010). Each data collection effort consisted of one high-resolution (0.03° by

Figure 2. Photograph of the largest rock fall that occurred on 26 August 2009, at 13:09 PST. Note location of Ahwhanee Hotel at bottom left. Photo by Nissen Jaffe. This figure is available in colour online at wileyonlinelibrary.com/journal/espl

0.03° angular resolution) laser scan from the same position on the ground, located approximately 640 m south of the rock fall source area. We typically collected three to six million points, each with a relative accuracy of 1 cm, providing nominal point spacing in the vicinity of the rock-fall source area of 30 cm.

We performed all registration, georeferencing, distance measurements, failure surface orientations, surface modeling, and area and volumetric analysis using I-SiTE Studio software (Maptek, 2011). We registered and georeferenced the initial terrestrial lidar data set for the Rhombus Wall (collected 5 September 2009) to the airborne lidar data (Figure 3) using approximately 1700 points with a mean registration error of 32 cm. We registered and georeferenced all subsequent terrestrial lidar data sets to the preceding terrestrial data set using approximately 3700 matching points with a mean registration error of 17 cm. Errors are greater for the first registration due to the lower cliff-face point density of the airborne lidar data. Distance measurements were performed using the point data in all cases; we estimate errors for these measurements to be on the order of 18 cm (17 cm mean registration error + 1 cm laser error). Orientations (dip/dip direction) of failure surfaces and local discontinuities were measured from the point data, with orientation uncertainties of approximately 1–2°.

Difference analysis of laser scanning data

We created interpolated surface models from lidar point clouds (Figure 4) using I-SiTE Studio's spherical triangulation algorithm, which is specifically designed for steep overhanging topography. Approximately 40 000 points were typically included in each triangulation over a cliff area of 10 000 m^2. Following a suite of surface consistency tests, we computed volume differences between triangulation surfaces, providing the total volumetric change between subsequent

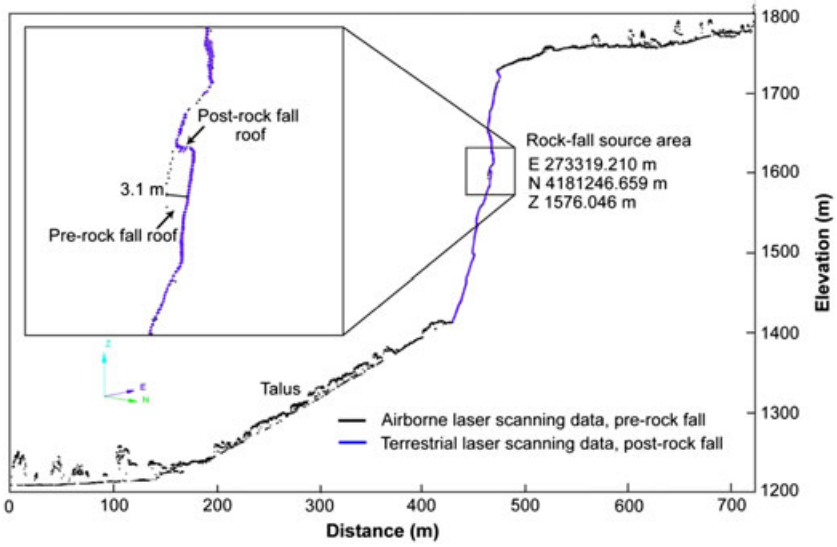

Figure 3. Cross-section through the Rhombus Wall area showing position and thickness of the slab that failed on 26 August 2009 by comparing airborne terrestrial laser scanning data collected before the rock falls (black) against terrestrial laser scanning data (blue) collected after the rock falls.

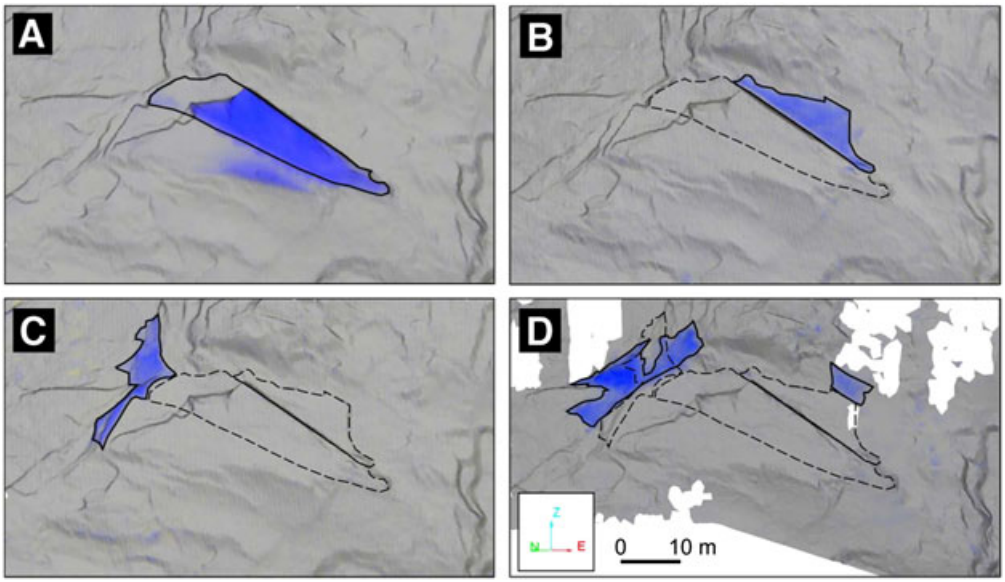

Figure 4. Difference analysis of interpolated surface models derived from airborne and terrestrial laser scanning data for the Rhombus Wall rock-fall source areas. Black lines delineate rock-fall perimeters (dashed for previous failures) and blue areas show areas of volume change between scans. (A) Failure area of the 26 August 2009 rock falls, with a cumulative volume of 740 m^3. Detected change below the source area is partially an artefact due to gaps in the airborne laser scanning data, but also represents some actual volume loss from a ledge below the source area due to impact of the main failure mass. (B) Failure area of the 14 September 2009 rock fall, with a volume of 108 m^3. (C) Failure area of the 30 August and 27 September 2010 rock falls, with a cumulative volume of 73 m^3. (D) Failure areas of the 28 October, 12 November, 13 November, and 20 November 2010 rock falls, with a cumulative volume of 110 m^3, are shown on the left; 14 m^3 rock fall that occurred at an unknown date is shown on the right. White areas in (D) represent cliff surfaces that were wet when scanned, scattering the laser and yielding poor data returns.

lidar data sets (Figure 4). For the 26 August 2009 rock falls, we computed volumes by differencing the airborne and terrestrial data sets; for subsequent rock falls, we computed volumes by differencing terrestrial data sets; errors associated with calculated total volumes vary between 7% for the largest rock fall (740 $m^3 \pm 52$ m^3, cumulative for all failures on 26 August 2009; Table I) to 25% for the smallest rock fall (4 $m^3 \pm 1$ m^3 on 23 December 2009; Table I). We then partitioned cumulative volumes into individual events (Table I) based on both photographic and lidar analysis and the contributing surface area for each rock fall.

Description of Events

Although the historical database of rock falls in Yosemite details several rock falls from the Rhombus Wall prior to August 2009, the particular source area that is the focus of this paper was not documented as active prior to 2009 (Wieczorek and Snyder, 2004, and additional unpublished observations). However, numerous cliff features such as overhangs and fan-shaped fracture textures (Bahat *et al.*, 1999) indicate that rock falls have previously occurred in this area prior to historical documentation. Furthermore, the extensive talus slope beneath the Rhombus Wall (Figure 1(B)) confirms that rock falls have been common at this location since deglaciation occurred at about 15–17 ka.

The first event of the Rhombus Wall rock fall sequence was a small rock fall that occurred at approximately 04:15 Pacific Standard Time (PST) on 26 August 2009 (area 1a in Figure 5). The rock fall was not witnessed directly given its early morning occurrence, but several residents living near the Rhombus Wall heard the impacts of falling rock onto the talus slope. A comparison of photographs taken later that morning at 07:30 PST

Table I. Temporal and spatial characteristics of the 2009–2010 Rhombus Wall rock falls

Event	Date	Time (PST)	Volume (m^3)	Mean thickness (m)	Surface area (m^2)	Failure surface orientation (dip°/dip direction°)
1a	26 August 2009	04:15	6[a]	3.1	2	72/216
1b	26 August 2009	12:30	19[a]	3.1	6	67/211
1c	26 August 2009	12:31	16[a]	3.1	5	68/214
1d	26 August 2009	12:31	78[a]	3.1	25	79/219
1e	26 August 2009	13:09	558[a]	3.1	180	79/213
1f	26 August 2009	14:35	60[a]	1.0	60	90/211
2	14 September 2009	17:12	108	0.8	135	80/214
3	23 December 2009	09:10	4	0.4	9	57/203
4	30 August 2010	01:45	30[a]	0.8	38	90/216
5	27 September 2010	13:30	43[a]	0.8	54	88/204
6	28 October 2010	20:05	33[a]	0.6	56	86/206
7	unknown	unknown	14	0.5	30	71/211
8	12 November 2010	16:42	40[a]	0.6	70	83/202
9	13 November 2010	12:04	28[a]	0.6	47	88/199
10	20 November 2010	22:55	2[a]	0.2	10	88/196

[a]Reported volumes are approximate and based on partitioning of cumulative failure volumes, derived from difference analyses of laser scanning data and failure surface areas revealed by high-resolution photographs and video.

with the gigapixel panoramic images of the Rhombus Wall acquired prior to the rock fall (Figure 1(B), 1(C)) reveals that the failure occurred at the inside corner of an alcove roof beneath an overhanging rock slab (area 1a in Figure 5; Figure 6). Stress concentrations can be expected at corners such as this in rock (Holister, 1967; Muller and Martel, 2000; Barber, 2002). The failure surface showed mostly freshly broken rock with ragged edges and no clearly defined pre-existing structural discontinuities. Local water staining on the newly exposed surface, however, indicates that a fracture behind the rock mass was open and conducting water, and had partially detached the rock mass from the cliff prior to failure.

Several hours later, beginning at approximately 12:30 PST, a series of three rock falls, separated in time by approximately 20–60 seconds, began at the initial failure area and propagated up and to the west (areas 1b, 1c, and 1d in Figure 5) along a sub-planar, near-vertical sheeting joint (Table I) that closely mirrored the orientation of the cliff face prior to failure. A park visitor captured the rock fall at 12:31 PST on high-definition video (Figure 7). Analysis of this video reveals a sudden distinctive ejection of rock dust just as a rock sheet begins to slip along the underlying sheeting joint surface, with associated tensile failure within the slab (Figure 7). The apparently explosive behavior indicates the presence and rapid redistribution of high stresses at the failure surface. The detached sheet subsequently slid down a steeply inclined face below the failure surface (dip/dip direction: 69°/217°) for ~20 m and then struck a bedrock ledge. The sheet fragmented into about 14 large pieces and free-fell approximately 140 m to the talus slope at the base of the cliff.

At 13:09 PST, a much larger rock fall occurred above and west of the earlier failures (area 1e in Figure 5), along the same sheeting joint surface. This slab had a volume of approximately 558 m^3, the largest of all of the 2009–2010 Rhombus Wall rock falls (Table I). This rock fall was widely documented by park visitors, employees, and residents throughout eastern Yosemite Valley (Figure 2). Rock debris, including boulders as large as 2 m in diameter, bounced and rolled to the base of the talus slope and damaged unoccupied vehicles in the parking lot of the Ahwahnee Hotel.

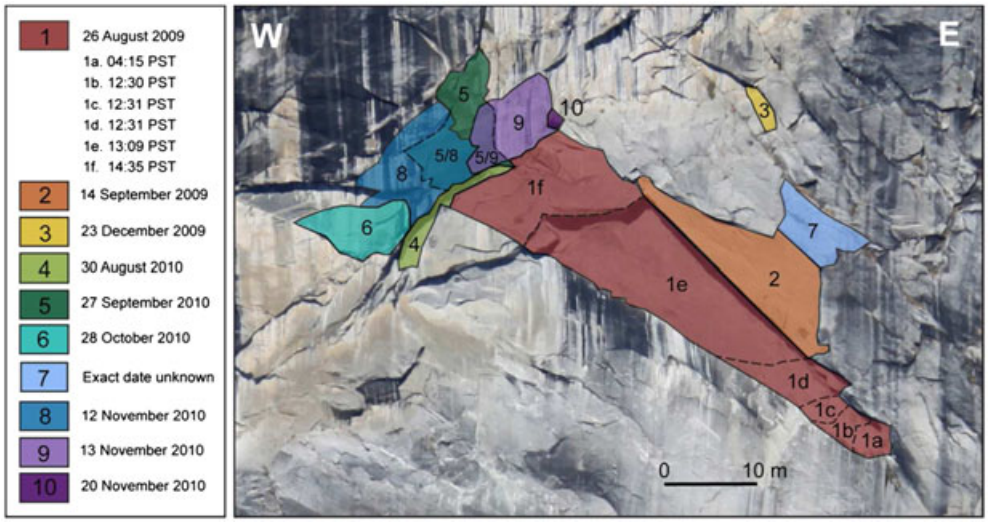

Figure 5. Spatial and temporal patterns of rock fall from the Rhombus Wall derived from observations, repeat digital photography, and repeat laser scanning. The failures progress in time from warm to cool colors, with red marking the first failures on 26 August 2009 and purple the most recent failure on 20 November 2010. Rock fall number 7 (light blue) was not documented at the time of occurrence, and thus lacks an exact date. Except for the failure of 23 December 2009 (yellow), all of the failures are adjacent to a previous failure, a pattern also revealed in the progressive failures of 26 August 2009 (red). These progressive failures are consistent with stress concentrations associated with a given fracture event initiating subsequent adjacent failures. This figure is available in colour online at wileyonlinelibrary.com/journal/espl

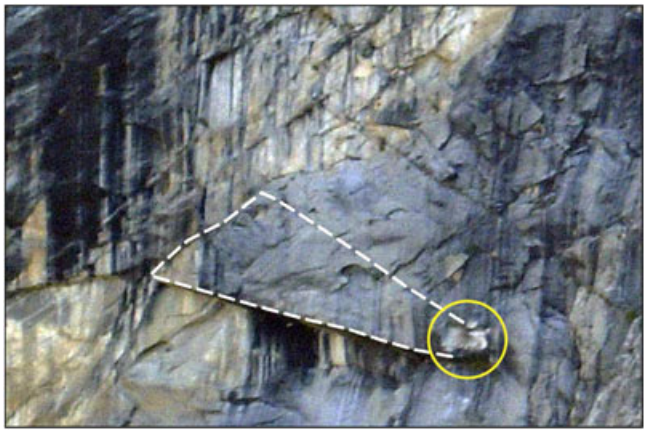

Figure 6. Photograph taken at 07:30 PST on 26 August 2009, following the first rock fall of the sequence (see area 1a in Figure 5). Comparison with high-resolution photographs taken prior to the rock fall (Figure 1(C)) highlights a small (5 m^3) failure (yellow circle) located at the tip of a triangular-shaped overhanging slab, a likely point of stress concentration. Subsequent failures later that day resulted in failure of the triangular slab (white dashed line). This figure is available in colour online at wileyonlinelibrary.com/journal/espl

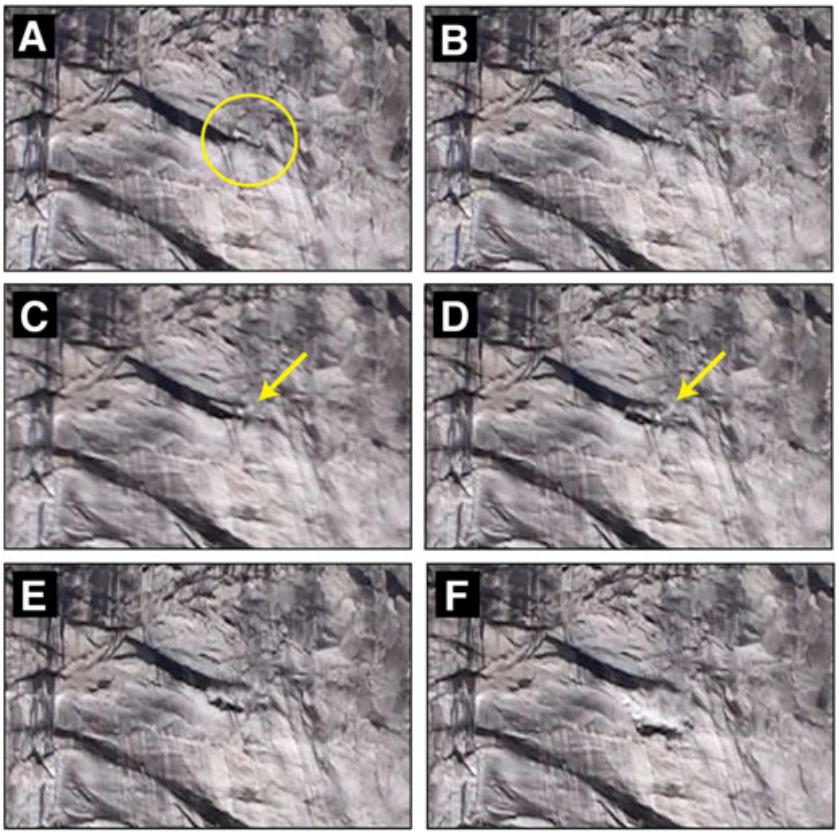

Figure 7. Image sequence showing detachment of 78 m^3 sheet at 12:31 PST on 26 August 2009 (area 1d in Figure 5). (A) Cliff surface immediately before detachment. Yellow circle marks detachment area. (B–D) Failure initiation, with forceful ejection of dust (yellow arrow) accompanying sudden slip along the underlying sheeting joint. Total elapsed time of image sequence is 1.2 seconds. Images from high-definition video taken by Robert Atkinson. This figure is available in colour online at wileyonlinelibrary.com/journal/espl

A smaller rock fall occurred at 14:35 PST (area 1f in Figure 5). Although this rock fall continued the progression of failures up and to the west, the failure surface 'stepped up' to a parallel sheeting joint that had formed shallower with respect to the cliff face; as a result, this rock fall consisted of a much thinner sheet than the failures earlier in the day (Table I).

The source area for all six rock falls occurring on 26 August 2009 was shaped like an inverted right triangle with a total surface area of 278 m^2 (Figures 5 and 6; Table I). The cumulative rock-fall volume was 736 m^3. The failed sheet had a mean thickness of 3.1 m over most of its length (Table I), consistent with calculations from overlapping cross-sections of airborne and terrestrial lidar data (Figure 3), but thinned to 1.0 m in the upper western corner where the last rock fall of the 26 August 2009 sequence occurred (Table I). The upper edge of the failure area was defined by a pre-existing discontinuity dipping moderately to the east-southeast (dip/dip direction = 38°/106°). Several discontinuities with similar orientations are present on the cliff face immediately above the failure area (Figure 8) and correspond to the 'J2' joint set prevalent in eastern Yosemite Valley (Wieczorek and Snyder, 1999; Wieczorek *et al.*, 2008; Matasci *et al.*, 2011; Stock *et al.*, 2011). Another set of discontinuities

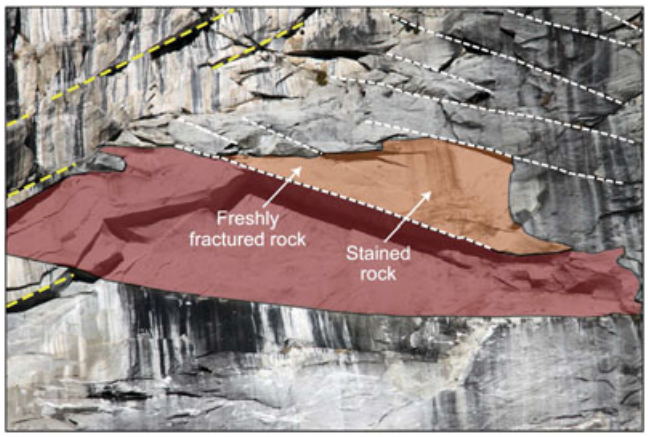

Figure 8. Photograph of the 14 September 2009 rock fall site (orange), which consisted of a thin (0.8 m) sheet located immediately above the failure area of the 26 August 2009 rock falls (red) and along a parallel surface. The 14 September rock fall occurred after approximately three weeks of audible cracking and visual observations of sheeting joint opening. Note the staining in the middle of the failure surface and the freshly fractured rock along the edge. White dashed lines mark moderately east-dipping discontinuities that dip moderately to the east and form the upper margins of failure surfaces. Yellow dashed lines mark discontinuities that dip moderately to the northwest.

that dip moderately to the northwest is present within and adjacent to the rock-fall source area, corresponding to the 'J20' joint set (Matasci *et al.*, 2011).

Over the next 3 weeks, cracking sounds were heard emanating from the Rhombus Wall from as far away as 1 km on at least four occasions, although they could not be definitively tied to the location of the 26 August 2009 rock falls. Visual monitoring from the ground and by helicopter during this period indicated that the aperture of a sheeting joint just beneath the cliff surface above the overhang created by the 26 August 2009 rock falls irreversibly widened by several centimeters. We interpret the cracking sounds and observed joint opening as occurring in response to fracture propagation along a sheeting joint behind the cliff surface above the new overhang created by the 26 August 2009 failures.

At 17:12 PST on 14 September 2009 a rock mass with a volume of 108 m^3 detached along the aforementioned sheeting joint. This joint was essentially parallel to the failure surface of the 26 August 2009 rock falls, but located at a much shallower depth (0.8 versus 3.1 m; Table I). The failure surface of the 14 September 2009 rock fall (area 2 in Figure 5) is an eastward continuation of the failure surface of the last rock fall that occurred on 26 August 2009 (area 1f in Figure 5). As with the earlier failures, the exposed failure surface showed some water staining, primarily near its center, with freshly fractured rock along the perimeter (Figure 8). Although the failure surface was dry when observed within 10 minutes after the rock fall occurred, the presence of water staining indicates that the sheeting joint was at least partially open and transmitting water behind the sheet for some time prior to failure (Figure 8).

The Rhombus Wall rock-fall source area was inactive for most of winter 2009 and spring 2010, except for a very small rock fall that occurred at 09:10 PST on 23 December 2009. This event was heard but not directly observed. Initial attempts to visually locate the source of this rock fall were unsuccessful, as the area immediately adjacent to the failure surfaces of 26 August and 14 September 2009 rock falls did not display obvious changes. Subsequent terrestrial laser scanning and difference analysis with the previous terrestrial scan revealed a small (4 m^3) volume change 12 m above the 14 September 2009 failure surface (area 3 in Figure 5). Because this rock fall did not share an adjacent surface with an earlier rock fall, and because it occurred during alternating wet and freezing conditions, we consider the possibility that this rock fall may not have been directly related to the earlier failures in 2009 and instead was a distinctly different event, like the many other small rock falls triggered by winter storms in 2009–2010. However, we cannot rule out the possibility that this rock fall was influenced by stress redistribution resulting from the 26 August and/or 14 September 2009 rock falls.

Rock-fall activity resumed at 01:45 PST on 30 August 2010 (area 4 in Figure 5), with failure generally progressing up and to the west. The failure involved a vertical slab of rock 0.8 m thick with a total volume of 30 m^3 on the western edge of the failure surface of the 26 August 2009 failures (Figure 5; Table I).

Approximately one month later, at 13:30 PST on 27 September 2010, a 0.8 m thick sheet 43 m^3 in volume (area 5 in Figure 5) detached from a position directly above the 30 August 2009 failure. This event reflects fracture propagation along the western margin of the failure area, predominantly upward behind the cliff face but also slightly to the west.

One month later, at 20:05 PST on 28 October 2010, another rock fall occurred from the far western margin of the failure area (area 6 in Figure 5). As with the previous rock falls from this area, the failed sheet was thin (0.6 m), with a total volume of 33 m^3 (Table I).

Approximately three weeks later, at 16:42 PST on 12 November 2010, another rock fall occurred along the western margin of the failure area (area 8 in Figure 5). This rock fall again involved a thin (0.6 m) rock sheet and had a volume of 40 m^3. The failure surface connected those of previous rock falls, and partially overlapped the failure surface of the 27 September 2010 rock fall (Figure 5). We interpret this overlap as progressive failure along stacked, thinly spaced sheeting joints with nearly identical orientations (dip/dip direction).

The following day at 12:04 PST, another rock fall occurred on the western margin of the failure area (area 9 in Figure 5). This rock fall, involving the same thin (0.6 m) sheet that failed the previous day, extended farther up the cliff. Its failure surface partially overlapped the failure surface of the 27 September 2010 rock fall (Figure 5). Cracking noises were heard from the Rhombus Wall approximately one hour prior to this failure, and the rock fall was widely witnessed throughout eastern Yosemite Valley.

The final rock fall of the 2009–2010 Rhombus Wall sequence occurred at 22:55 PST on 20 November 2010. This failure (area 10 in Figure 5), which had a volume of approximately 2 m^3 (Table I), involved a very thin (0.2 m) sheet located on the eastern side of the 13 November 2010 failure.

Difference analysis following a terrestrial laser scan on 14 December 2010 revealed one additional rock fall that had not been previously documented (area 7 in Figure 5). This failure consisted of a thin (0.5 m) sheet with a volume of 14 m^3, located above the 14 September 2009 failure surface (Figure 5). Repeat photographs show that this sheet was in place on 28 October 2010, but missing on 12 November 2010. Although there were no reports of rock falls from the Rhombus Wall during this time, many small rock falls that occur in Yosemite Valley are not reported. Perhaps this sheet also failed on 12 November 2010, along with area 8 on the western margin (Figure 5), but we are unable to test that possibility with the available data. Therefore, we cannot identify an exact date or time for this rock fall (Table I). However, its position adjacent to an earlier failure, and its occurrence during a period of high rock-fall activity on the Rhombus Wall, strongly suggest that it was related to the other failures. This failure was interesting in that it occurred on the eastern side of the rock-fall source area after a hiatus in activity on that side of more than one year.

Five important observations result from detailed documentation of these events: (1) each rock fall was a temporally distinct event, separated in time from earlier failures by approximately 20 seconds to eight months; (2) all of the rock falls involved failures of thin sheets along nearly planar fractures with similar orientations that roughly parallel the pre-rock fall cliff surface (Table I); (3) all but two of the fifteen rock falls either overlapped or occurred along the perimeter of at least one previous failure surface (Figure 5), the exceptions being the initial event (area 1a in Figure 5) on 26 August 2009 and the small rock fall on 23 December 2009 (area 3 in Figure 5); (4) some of the rock falls were associated with cracking sounds, and in one case with visible sheeting joint opening; and (5) the thickness of the failed sheets decreased as the rock-fall sequence progressed in both time and space. These observations indicate that the rock falls were related through a time-dependent process of progressive failure along sheeting joints commonly bounded by regional discontinuities.

Potential Rock-fall Triggering Mechanisms

Considerable effort has been expended to identify and analyze specific triggering mechanisms for rock falls in Yosemite

(Wieczorek and Jäger, 1996; Wieczorek and Snyder, 2004; Wieczorek *et al.*, 2008). Although many rock falls are temporally correlated with specific meteorological events such as rainfall, snowmelt, or freeze–thaw events, or with seismically induced ground shaking, these temporal correlations do not always point to a clearly defined mechanical trigger. Furthermore, many rock falls cannot be reliably correlated with such 'recognized' triggers, even when closely observed. Thirty-three percent of all documented rock falls in Yosemite are reported as having 'unrecognized' triggers (Wieczorek and Snyder, 2004, and additional unpublished observations). Such an absence of recognized triggers, while not unusual (Sanderson *et al.*, 1996), probably reflects incomplete understanding of subtle changes that can occur along discontinuities.

The 2009–2010 Rhombus Wall rock falls occurred over a wide variety of meteorological conditions, and many of the rock falls cannot be temporally correlated with a recognized triggering mechanism. The rock falls on 26 August 2009 revealed some seepage on the failure surface, but it is unclear whether this water triggered these failures or whether the failure occurred for other reasons and simply revealed seepage that was present beneath the failed sheet. Most of the subsequent rock falls from the Rhombus Wall were dry failures, suggesting that water did not act as a trigger. Dry failures are relatively common in granitic landscapes with sheeting joints, and might be related to diurnal and/or annual changes in temperature and/or humidity (Chau and Shao, 2006; Vargas *et al.*, 2009; Nara *et al.*, 2010); it is interesting to note that most of the Rhombus Wall rock falls occurred during what are typically warm and dry months in Yosemite Valley (August through November; Table I). In any case, the time-dependent progressive nature of these rock falls is not easily attributable to elevated water pressures. Considering the many rock falls in Yosemite Valley (and elsewhere) that lack recognized triggers, we suggest that a rock fall might not have an easily recognizable trigger if the failure process involves subcritical crack propagation (Bahat *et al.*, 1999).

Our visual observations, high-resolution photographs, and lidar data analyses demonstrate that the majority of failure surfaces for the 2009–2010 Rhombus Wall rock falls were formed by interconnected sheeting joints (Figure 5; Table I). The characteristic presence of water stains on the failure surfaces demonstrates that most of the joints behind the failed sheets were at least partially open and conducting water prior to failure (Figure 8). However, observations that many of the failed slabs were bounded on the top by regional discontinuities, and that many failure surfaces exhibited freshly fractured rock along the perimeters (Figure 8), suggest that the failed slabs were attached at their margins prior to failure.

As presented in the Introduction, time-dependent failure of rock slopes can occur for several reasons, including weathering of failure surfaces, subcritical crack growth, and fracture propagation through intact rock bridges (Einstein *et al.*, 1983; Atkinson, 1984; Eberhardt *et al.*, 2004; Kemeny, 2005; Kim and Kemeny, 2009). These processes might have contributed to the Rhombus Wall rock falls. However, the observations described above suggest that the Rhombus Wall rock falls were fundamentally related to sheeting joints formed (sub)parallel to the surface, and perhaps involved the propagation of these joints into areas of previously intact rock. Below, we examine the mechanics of sheeting joint propagation to gain insight into the stresses around the Rhombus Wall and the role stress concentrations associated with sheeting joints might have played in triggering the progression of rock falls from the Rhombus Wall.

Mechanical Analysis of Sheeting Joint Propagation

Our conceptual model for the involvement of sheeting joint propagation in the Rhombus Wall rock falls is based on several key field observations:

(1) Sheeting joints are opening-mode fractures that develop (sub)parallel to a rock face (Martel, 2006, 2011).
(2) The near-parallelism of sheeting joints to current topographic surfaces, the presence of thin, loose rock slabs bounded by sheeting joints in areas recently scoured by glaciers, and related field observations indicate that many sheeting joints in Yosemite are geologically young, with some nucleating, opening, and propagating historically (Martel, 2006, 2011, and references therein).
(3) The cliff face and a (sub)parallel sheeting joint constitute essentially the entire front and back, respectively, of each rock slab that separated and fell during the 2009–2010 Rhombus Wall rock falls. Given the similar geometries and failure surface orientations of the slabs (Table I), sheeting joints appear to be essential contributors to the Rhombus Wall rock falls.
(4) The presence of freshly fractured rock either along or at the margin of sheeting joints at the Rhombus Wall rock-fall source area indicates that fracturing during the initial stages of failure involved sheeting joints.

Since the rock fracture process involves the nucleation, propagation, and termination of fractures (Lawn, 1993), the observations above suggest that the Rhombus Wall failures might have involved the propagation of sheeting joints in-plane into pre-existing regional discontinuities, and/or out-of-plane either to the cliff surface or into pre-existing regional discontinuities. To examine the factors that cause sheeting joints to open and propagate parallel to a cliff face at shallow depths, and to evaluate the role this process may have played in the Rhombus Wall rock falls, we considered the mechanics of three salient aspects of the failures: (1) the stresses that drive the propagation of sheeting joints and hence trigger rock falls; (2) sheeting joint geometry, which then dictates the geometry of the rock falls; and (3) the progressive nature of the failures.

Stresses that drive sheeting joints

Martel (2006, 2011) proposed that tensile stresses perpendicular to a cliff face are necessary for sheeting joints to nucleate, open, and propagate. The source of such a tension has been unclear, but a plot of the normal stress T perpendicular to the surface of a traction-free slope as function of distance normal to the slope z shows how a tension might occur (Figure 9). Accordingly, if the slope of the T vs. z curve at a traction-free surface is ϕ, and if ϕ is positive, then T must be tensile (positive) at shallow depths (Figure 9). A positive stress gradient ϕ can be generated by compressive stresses parallel to a cylindrical ('two-dimensional') traction-free rock slope if it is convex, even for gentle slopes (Martel, 2006); for surfaces of arbitrary shape the surface must be convex in at least one direction (Martel, 2011). For two-dimensional surfaces, the stress gradient ϕ is given by:

$$\left.\frac{dT}{dZ}\right|_{z=0} = \phi = kP - \rho g \cos\beta \qquad (1)$$

where k is the curvature of the surface (negative where convex), P is the normal stress parallel to the surface (compression is

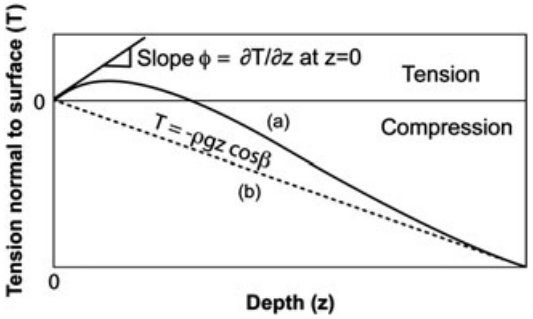

Figure 9. Schematic diagram showing possible variations in the normal stress T perpendicular to a traction-free rock surface as a function of distance into the surface z. The stress gradient ϕ is the slope of the T vs. z curve at the surface. (a) General form of stress profile required for sheeting joints, with a tensile stress at shallow depth and $\phi > 0$. (b) Linear stress profile for a constant gravitational stress gradient for a flat slope inclined at an angle $\beta < 90°$, with $\pi < 0$. Tension is positive, compression is negative. Modified from Martel (2011).

negative), ρ is the density of the rock, g is gravitational acceleration (9.8 m/s^2), and β is the topographic slope angle in degrees (Martel, 2006). The gradient thus has contributions from both a curvature-stress term (kP) and a gravitational term ($-\rho g \cos\beta$). A tensile stress normal to a two-dimensional rock face will be present in the shallow subsurface (Figure 9) if

$$kP > \rho g \cos\beta \tag{2}$$

For steep slopes such as the walls of Yosemite Valley in general, and the Rhombus Wall in particular, the slope is locally vertical or close to it, $\beta \to 90°$, so the cosine terms on the right side of Equations (1) and (2) above become small, and the gravitational gradient term essentially drops out. As a result, ϕ is positive and tensile stresses will exist behind steep convex slopes ($k < 0$), since the stress parallel to the slope P must be compressive due to the weight of the rock that forms the slope. At overhanging slopes $\beta > 90°$ and $\cos\beta < 0$, so the gravitational gradient term in Equation (1) actually increases the normal stress gradient further. Tensile stresses are thus very likely to be present normal to the face of a steep convex cliff. Since rocks are weak in tension, a sustained tension perpendicular to the surface a short distance behind or beneath a rock face can be expected to open sheeting joints that parallel the rock face. Thus, both steep convex slopes and overhanging slopes can contribute to the opening (propagation) of sheeting joints. These conditions exist at the Rhombus Wall rock-fall source area (Figure 3), as well as at many other places in Yosemite Valley.

The mechanism described above explains how a tensile stress normal to a cliff face could be generated to yield a sheeting joint with a surface area of many square meters. In the absence of a tension normal to the cliff face, a compressive stress parallel to the cliff face, by itself, could give rise to localized tensile stresses associated with grain-scale heterogeneities, flaws, and voids, but these localized grain-scale effects cannot account for sheeting joints with the observed dimensions at the Rhombus Wall (Table I; Nemat-Nasser and Horii, 1982). We therefore conclude that the tension induced by the surface curvature contributes fundamentally to the formation of sheeting joints.

Using information on the geometry of the Rhombus Wall derived from the lidar data, we can calculate the value of the minimum stress gradient at the Rhombus Wall prior to failure. If we assume a uniform rock density and assume that P were due exclusively to the component of the weight of the rock that acts parallel to the average slope β^* above a point of failure, then

$$kP = k\rho g h \sin\beta* \tag{3}$$

where h is the height of the cliff above the point being evaluated. Using the lidar-derived curvature of the profile of the cliff at the Rhombus Wall rock-fall source area prior to failure of about 0.05 m^{-1}, a rock density of 2.7×10^3 kg/m^3, a value of h of 126 m (see Figure 3), and a value for β^* of 85°, the stress gradient term on the left side of Equation (3) is 2×10^5 Pa/m. This is the minimum value of the kP term on the left side of inequality (2) because tectonic stresses and thermal stresses also can contribute to P. Compressive stresses of ~6–21 MPa have been measured parallel to the surface in two places in Yosemite National Park along much gentler slopes than the cliffs of Yosemite Valley (Cadman, 1970; Hickman *et al.*, 1993). We expect that the surface-parallel stresses along the cliff faces, where gravitational stresses increase the surface-parallel stresses, are likely to be at least as large as those measured on gentle slopes. The actual value of the kP term on the left side of inequality (2) thus could be several times larger than 2×10^5 Pa/m. The right side of inequality (2) has a maximum possible value of $+2.6 \times 10^4$ Pa/m (if $\cos\beta = 1$), but at the Rhombus Wall the value will probably be about an order of magnitude smaller since $\cos\beta = 0.1$; locally it will even be negative. Regardless, the criteria for a tensile (positive) stress gradient at the surface clearly are met at the Rhombus Wall, so the presence of sheeting joints there is accounted for by this analysis.

To describe the stresses around an isolated sheeting joint, we use a right-handed reference frame where the x-axis extends into the page, the y-axis parallels the cliff face and points up, and z-axis is normal to the cliff face and points into the cliff (Figure 10). From this point on in our analyses we ignore the *actual* curvature of the cliff face and the sheeting joint and treat both as planar (Figure 10). We do, however, account for the *effect* of the curvature of the cliff face by including not only the compressive stress parallel to the cliff face ($P = \sigma_{yy}$), but also the associated tensile stress perpendicular to the rock face ($T = \sigma_{zz}$) induced by the curvature. This treatment means that our solution is approximate, not exact, because neither the crack nor the surface in our model is curved. For simplicity we consider T in the ambient stress field to be constant along the eventual plane of the crack ($z = d$), designating the ambient value of T along the plane of the crack as T^c, with $T^c > 0$ (Figure 10). No displacements are allowed in the x-direction, and the shear stresses σ_{zx} and σ_{yx} are considered to be zero. The stress state is thus one of plane strain (Timoshenko and Goodier, 1970).

Our formulation of the elastic boundary value problem to examine how sheeting joints propagate utilizes the principal of superposition. We treat the host rock as a homogenous, isotropic, isothermal, linear elastic material with Young's modulus E and Poisson's ratio ν. We consider the total stress field (Figure 10(A)) as the superposition of an ambient stress field (Figure 10(B)) that exists in a crack-free body bounded by a traction-free surface, and the stress perturbation associated with the opening of a crack of half-length a in an otherwise unloaded body bounded by a traction-free surface (Figure 10(C)). In the parlance of differential equations, the ambient stress field is a particular solution of the governing differential equation of elasticity theory, and the stress perturbation is a complementary solution (Martel, 2000). The stress field for the perturbation is precisely equivalent to the stress field for a pressurized crack in a half-space, the case considered by Pollard and Holzhausen (1979). To obtain the

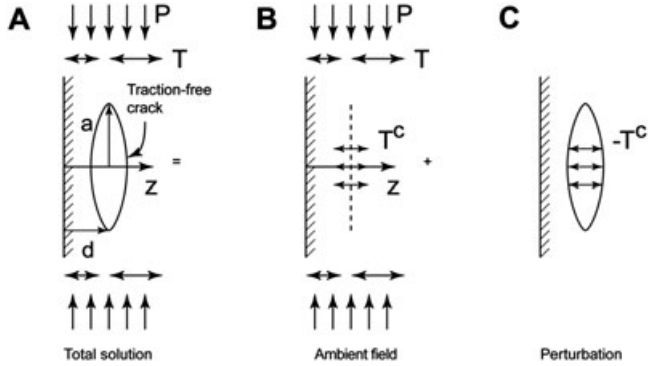

Figure 10. Superposition scheme for stresses around a sheeting joint parallel to a cliff face, showing the reference frame. The z-axis is normal to the slope, the y-axis points upward, parallel to the slope, and the horizontal x-axis points into the page. (A) Traction-free crack of half-length a at a depth d behind a traction-free rock face. (B) Assumed ambient stress state in the absence of a crack. The tensile stress T normal to the rock face is assumed to increase over a short distance from the face, and compressive stresses parallel to the rock face is P. The value of T at depth z is positive and equals T^c. (C) Pressurized crack, with an internal pressure $-T^c$; the minus sign is required because pressure is taken to be negative. The total stress field (A) is the sum of the ambient stress field (B) and the stress perturbation due to the opening of the crack (C).

required traction-free boundary condition along the walls of the crack, the pressure in the crack must have the same magnitude as the tension in the ambient field at the depth of the crack, but the opposite sign (Figure 10(C)). Superposition of the two stress fields in Figure 10(B) and 10(C) thus describes the stress about a crack that is traction-free (Figure 10(A)). If the ambient tension at depth d is T^c, then the normal traction on the crack walls in the perturbation solution is $-T^c$ (Figure 10). For shallow depths beneath a traction-free surface, an approximate value for T^c is obtained by the product of the stress gradient, given in Equation (1), and the depth below the surface d (Figure 9):

$$T^c = T(z=d) \approx \left[\left.\frac{dT}{dz}\right|_{z=0}\right][d] = [kP - \rho g \cos\beta][d] \quad (4)$$

Key fracture mechanics concepts

To gain insight into the propagation tendencies of sheeting joints, we apply principals of linear elastic fracture mechanics (Pollard and Segall, 1987). In fracture mechanics, the stress field near the tip of a crack has the following closed form solution (e.g., Lawn, 1993):

$$\sigma_{ij} = \frac{K_m}{\sqrt{2\pi r}} f_{ij}(\theta), \quad (5)$$

where σ_{ij} is the stress component acting on a plane normal to the i-direction, and acting in the j-direction, K_m is the stress intensity factor, r is a small distance from the fracture tip ($r << a$), and f_{ij} is a trigonometric function of the angle θ (Figure 11). Note that the stresses are singular (i.e. they approach infinite levels as $r \to 0$), and that the contribution of the angular component of position θ is separable from that due to the radial component r. The subscript m denotes the mode of fracturing (i.e. the style of relative motion of the crack walls near the fracture tip), with m = I for the opening mode, and m = II for sliding modes (Figure 12). For a mixed-mode crack, both opening and sliding can occur. The displacement of the crack walls relative to one another Δu_m near the crack tip also can be expressed in terms of the stress intensity factor (Lawn, 1993)

$$\Delta u_m = C\left(\frac{K_m}{2E}\right)\sqrt{\frac{r}{2\pi}} \quad (6)$$

where C is an elastic constant. In elastic materials, the stresses are proportional to the strains, and the strains come from derivatives of the displacements with respect to position. Relative displacement near the crack tip varies as $r^{1/2}$, consistent with the stresses varying as $r^{-1/2}$.

Equations (5) and (6) show that the stresses and relative displacements near the tip of a crack are proportional to the stress intensity factor. Accordingly, as the stress intensity factor increases, so does the propensity of the fracture to propagate (Lawn, 1993). The stress intensity factor depends on the crack geometry and the boundary conditions of the problem. The mode I stress intensity factor K_I for an isolated pressurized two-dimensional crack of half-length a in an infinite body with no ambient stresses is:

$$K_I = \Delta\sigma\sqrt{\pi a}, \quad (7a)$$

whereas for a three-dimensional penny-shaped crack of radius a, K_I is given by:

$$K_I = \frac{2}{\pi}\Delta\sigma\sqrt{\pi a}, \quad (7b)$$

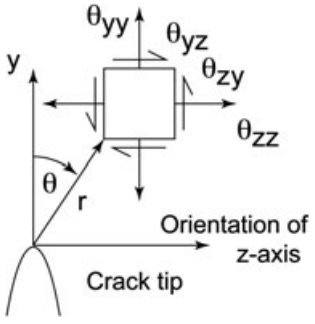

Figure 11. Reference frame for stresses near the tip of a crack. Positive stresses are depicted.

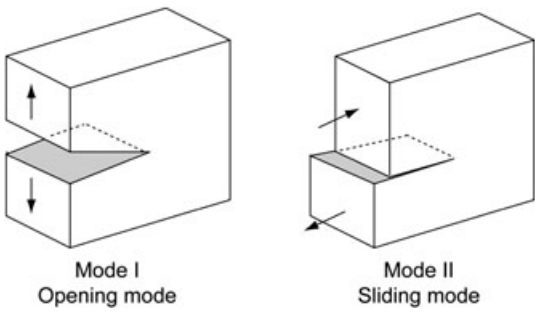

Figure 12. The two modes of fracturing in plane strain.

(Lawn, 1993). In both cases $\Delta\sigma$ is the driving pressure:

$$\Delta\sigma = \sigma_{zz}^{ambient} - \sigma_{zz}^{crack\ \ walls} \tag{8}$$

The half-length or radius a thus defines the crack geometry, and the driving pressure $\Delta\sigma$, which equals T^c here, comes from the boundary conditions of the perturbation problem (Equation (4); Figure 10(c)). The similar forms of Equations (7a) and (7b) indicates that an analysis of a two-dimensional crack can also provide at least qualitative insight into the behavior of a three-dimensional penny-shaped crack that resembles a sheeting joint.

We note that the stress intensity factor for a traction-free crack under tension (Figure 10(A)) can be the same as for a pressurized crack (Figure 10(C)). This is because the driving pressures can be the same, even though the stress fields far from the cracks can be very different. In other words, the conditions at the tips of a crack opening in tension can be indistinguishable from those at the tips of a pressurized crack. The behavior of a pressurized crack thus is useful in understanding propagation of a dry sheeting joint.

Propagation paths for sheeting joints

The relative displacement of the walls of a rock fracture near its tip can be used to predict the propagation paths of the fracture. Equation (6) shows that the stress intensity factors can be used to describe the near-tip relative displacements, hence the predicted propagation paths can be couched in terms of stress intensity factors.

The mode II stress intensity factor K_{II} describes near-tip conditions in cases where crack walls slip by one another. For an isolated pressurized crack in an infinite body with no ambient stresses, $K_{II}=0$. This occurs even though tangential displacements do occur along the crack walls (Figure 13), but these displacements are matched such that no tangential displacement of the walls occurs *relative to one another*; the displacements are symmetric about the plane of the crack. For a pressurized crack near a traction-free surface, however, the displacements are asymmetric (Figure 13(B)). The displacements normal to the plane of the crack are larger on the crack wall nearer to the free surface than along the opposing wall. Furthermore, the tangential displacements also are larger on the crack wall nearer to the free surface than along the opposing wall (i.e., $u_y^- > u_y^+$). This means a relative tangential displacement of the walls occurs because of a mechanical interaction between the crack and the traction-free surface. As a result, for a pressurized crack near a traction-free surface, $K_{II} \neq 0$. This has important ramifications for sheeting joint propagation.

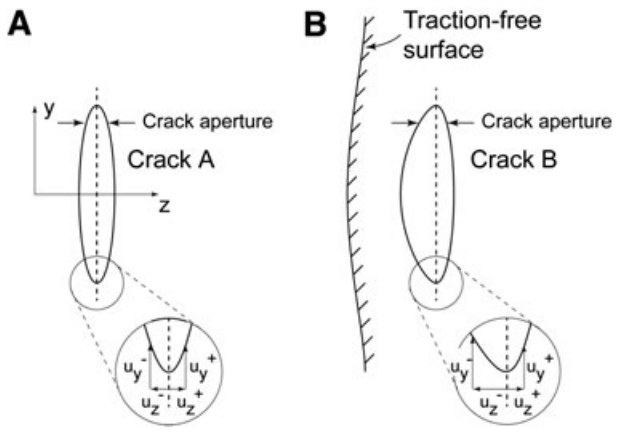

Figure 13. Displacements of the walls of a uniformly pressurized crack (A) in an infinite body, and (B) in a half-space. The aperture is greater for crack B than for crack A owing to the proximity of the free surface. Crack opening includes displacement components (fine arrows in inset) tangential to the crack (u_y) as well as normal to the crack (u_z). The dashed line shows the walls of the crack prior to pressurization. The positive walls of the crack are to the right of the dashed line, the negative sides to the left. The asymmetry in the normal displacements for crack B is also associated with an asymmetry in the tangential displacements, with $uy^- = uy^+$ in (A), but $u_y^- > u_y^+$ in (B). The sense of slip at the upper end of the crack is opposite the sense of slip at the lower end.

The influence of the proximity of a free surface on a pressurized crack can be quantified through the stress intensity factors. Dyskin *et al.* (2000) describe an asymptotic method for evaluating K_I and K_{II} for a two-dimensional pressurized crack parallel to a traction-free surface. In their procedure, the stress intensity factors (both K_I and K_{II}) for a crack parallel to a traction-free surface are normalized by the value of K_I for a crack of equal half-length in an infinite body. The right half of (Figure 14(A). shows that, for a half-length less than the depth, the normalized values of K_I effectively equal unity and the normalized values of K_{II} effectively equal zero. This means that sheeting joints essentially do not feel the effect of the traction-free surface if their shortest half-dimension is less than the depth of the crack below the surface. If a crack continues to grow, then the absolute value of K_I increases because the half-length a increases (see Equations 7). A positive feedback thus promotes further crack propagation. Moreover, the left half of Figure 14(A) shows that the normalized values of both K_I and K_{II} increase as the ratio of depth to half-length decreases, which will happen as the crack grows. This means a crack parallel to a traction-free surface would tend to propagate more readily than an isolated crack in an infinite body.

The ratio K_{II} / K_I provides a measure of the tendency of a fracture to deviate out of the plane tangent to the fracture at the fracture tip (Pollard and Aydin, 1984). If K_{II} / $K_I = 0$, then the fracture is expected to propagate in the tangent plane, but if this ratio departs from zero, the fracture is expected to deviate out-of-plane if it propagates (Lawn, 1993). Figure 14(B) shows that as the depth to half-length ratio decreases, which would happen as a sheeting joint propagates, the ratio K_{II} / K_I increases; this increase is particularly pronounced as the depth to half-length ratio drops below a value of unity. Thus, sheeting joints with in-plane dimensions greater than the fracture depth can be expected to propagate out of plane, and to grow towards the surface (Erdogan, 1971; Pollard and Holzhausen, 1979). The general tendency is for the fractures to grow in a direction that minimizes the shearing stresses resolved across the tips and maximizes the so-called hoop stress, the normal stress perpendicular to a radial plane extending from the crack tip (Figure 14(C)). The crack tip thus re-orients itself to grow as a mode I fracture and minimize the value of K_{II} at the fracture tips (Lawn, 1993). This suggests that sheeting joints, as they grow, will tend to daylight (intersect the cliff face), completely separating a relatively thin sheet of rock from a slope; on a steep cliff face, this separation would result in a rock fall. Thus rock falls could occur without a sheeting joint propagating into pre-existing discontinuities to allow a rock mass to separate from a cliff. Although many of the Rhombus Wall failure surfaces did terminate along pre-existing regional discontinuities (Figure 8), there are also examples where failure surfaces appear to have daylighted on the cliff face (e.g. the 14 September 2009 and 12 November 2010 rock falls).

In addition, the tendency for a sheeting joint to propagate towards the surface reflects a greater tensile stress concentration between the tip of the joint and the cliff face than on the

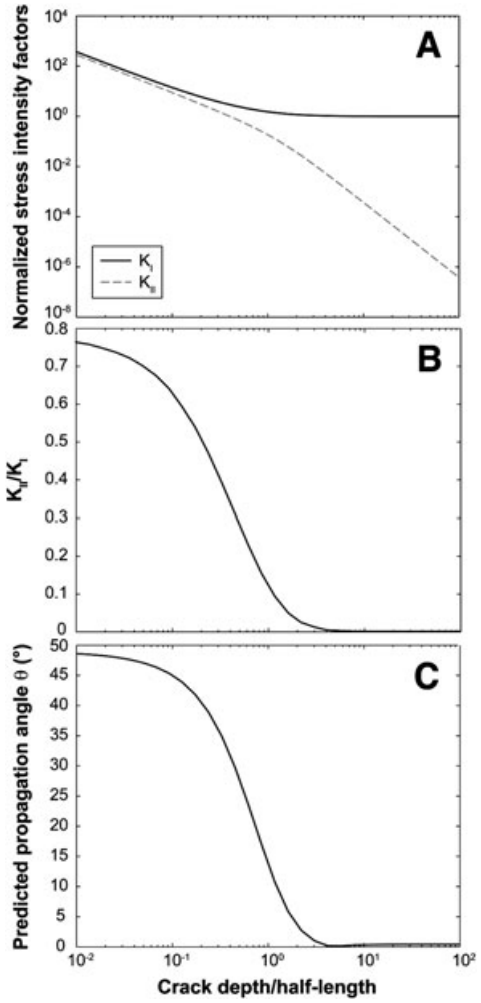

Figure 14. (A) Normalized stress intensity factors K_I (mode I) and K_{II} (mode II) for a uniformly pressurized two-dimensional planar crack parallel to a traction-free surface as a function of the depth/half-length ratio of the crack. The stress intensity factors are normalized by K_I for a uniformly pressurized crack in an infinite body. Stress intensity factors are calculated by the approach of Dyskin *et al.* (2000). (B) Ratio of K_{II} to K_I as a function of the depth/half-length ratio of the crack. (C) Predicted initial crack propagation angles as a function of the depth/half-length ratio of the crack. A value of zero corresponds to propagation in plane.

side of the joint away from the cliff face. Thus, if the stress concentration at the tip of a sheeting joint is able to help drive propagation of other nearby sheeting joints, the joints closer to the surface will be favored. This could account for the tendency of failures at the Rhombus Wall to occur progressively closer to the cliff face, resulting in progressively thinner slab failures through time (Table I).

Propagation geometry of sheeting joints

The analysis so far suggests that sheeting joint failures should involve rock sheets no more than a few times longer than they are thick. The actual failed sheets at Rhombus Wall, however, are typically at least several times longer than they are thick; for example, the 14 September 2009 failure had a maximum length of 31 m compared with a thickness of only 0.9 m (Table I). We attribute this discrepancy to strong compressive stresses parallel to the cliff face, and note that such stresses can exist even in situations where notches or overhangs exist on the cliff face (Figure 15).

The propagation of a sheeting joint up towards the surface can be considered as a consequence of slip that occurs near its tips due to a mechanical interaction with the cliff face (Figure 16(A)). Once a sheeting joint begins to propagate up towards the cliff face, however, a shear stress of the opposite sense is resolved across the new tip of the sheeting joint (Figure 16(B)); this occurs because the new tip is oblique to the ambient principal stresses *P* and *T*, which differ substantially in magnitude. As a result, the joint will tend to propagate back in a direction perpendicular to the most tensile stress (cf. Pollard and Aydin, 1984; Olson and Pollard, 1989). The strong anisotropy in the ambient stress field thus tends to 'steer' joints back to a path parallel to the cliff face. This anisotropy apparently is sufficient to allow sheeting joints to grow to lengths many times greater than their depth, as revealed by the failed sheets on the Rhombus Wall (Figure 5; Table I). This accounts for the characteristic tendency of slabs bounded by sheeting joints to be thin relative to their in-plane extent.

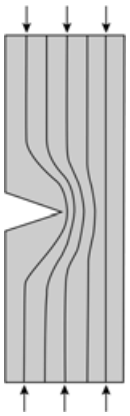

Figure 15. Stress trajectories parallel to the most compressive stress in a notched bar subject to uniaxial compression (modified from Holister, 1967). The notched bar is analogous to a cliff with an overhang. The trajectories are subparallel to the surface of the bar, even near the overhang above the notch. The trajectories near the convex corners show the approximate paths that opening-mode fractures would propagate along if the induced tensile stresses near the convex corners were sufficient to open cracks.

If a planar fracture propagates under a sustained tensile stress, the mode I stress intensity factor will increase as the fracture grows (Equation (7)). Similarly, if both the mode I and mode II stress intensity factors increase as a slightly curved or kinked fracture grows, its effective mode I stress intensity factor will increase (Cotterell and Rice, 1980). Provided the stress intensity factor (or effective stress intensity factor) remains below a critical level (Lawn, 1993), the sheeting joint can propagate in a stable, subcritical manner. We interpret the cracking noises at the Rhombus Wall as reflecting this type of crack growth. Once the stress intensity factor reaches a critical level, however, a fracture propagates spontaneously and the adjacent rock slab fails. We interpret the rather abrupt onset of failure at the Rhombus Wall as reflecting critical crack growth immediately prior to and during failure.

Progressive nature of sheeting joint failures

The final point we address here is the progressive nature of the Rhombus Wall rock falls. We recognize two key factors that can account for progressive failure of this type. First, several of the Rhombus Wall failures occur where a sheeting joint intersects a pre-existing regional discontinuity, usually at a high angle (e.g., Figure 8). These intersections tend to form sharp topographic corners that are expected to have strong stress concentrations (Muller and Martel, 2000; Barber, 2002). This can promote the development of new sheeting joints. Second, our

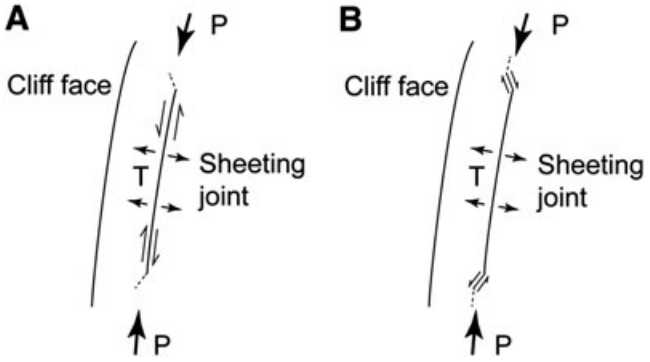

Figure 16. Schematic diagram showing sheeting joint propagation paths within a cliff. Dashed line shows the path of the sheeting joint during a subsequent stage of growth. (A) Sheeting joint propagates towards cliff face in response to shearing induced near joint ends as a result of mechanical interaction with the cliff face. (B) Sheeting joint propagates parallel to cliff face in response to shearing induced near new joint ends in response to the ambient principal stresses, defined by *P* and *T*.

observations of water stains emanating from the inside corners of overhangs, as well as observations of sheeting joint surfaces visible after rock falls occur, demonstrate that in some cases sheeting joints extend past the corners, so the actual tip line of a joint might be concealed. A strong stress concentration can be expected near the concealed tip line. Either or both of these situations can contribute to subsequent rock falls near the margin of a previous failure. As a region of failure spreads across a cliff face, the stress concentrations associated with previous failures will tend to spread with it, setting the stage for further failures. We consider the progressive failures from the Rhombus Wall to be a possible example of this type of stress redistribution.

Conclusions

Detailed monitoring of the 15-month-long sequence of rock falls from the Rhombus Wall in Yosemite Valley, aided by high resolution photography and laser scanning, yields five important observations: (1) each rock fall was a temporally distinct event, separated in time from earlier failures by approximately 20 seconds up to eight months; (2) all of the rock falls involved failures of thin sheets along nearly planar fractures with similar orientations that roughly parallel the pre-rock fall cliff surface; (3) after the initial failures in August 2009, all but one of the fourteen subsequent rock falls either overlapped or occurred along the perimeter of at least one previous failure surface; (4) some of the rock falls were associated with cracking sounds, and in one case with visible sheeting joint opening; and (5) the thickness of the failed sheets decreased as the rock-fall sequence progressed in both time and space. These observations indicate that the rock falls were related through a time-dependent process of progressive failure along sheeting joints commonly bounded by regional discontinuities.

Our mechanical analysis of the Rhombus Wall rock falls yields the following salient results: (1) cliff geometry dictates that tensile stresses should occur perpendicular to a steep, convex cliff face; (2) stress intensity factors indicate that sheeting joints should propagate parallel to a cliff face, with high compressive stresses parallel to a cliff face allowing a sheeting joint to propagate parallel to the cliff over distances many times the joint depth; and (3) asymmetric stress concentrations at crack tips promote crack propagation and ultimately destabilize a cliff face, triggering rock falls and setting the stage for further failures along the fracture periphery. Thus, a progressive sequence of rock falls occurring over a range of meteorological conditions need not be explained by a variety of triggering mechanisms but instead might result solely from the time-dependent propagation of cracks due to stress redistribution following a previous rock fall. The 2009–2010 Rhombus Wall rock falls are the best-documented example of a progressive rock fall in Yosemite Valley thus far, but several earlier rock falls exhibited similar tendencies and might have also involved sheeting joint propagation (Wieczorek and Snyder, 1999, 2004; Stock *et al.*, 2011).

Although our analysis focuses on the Rhombus Wall rock falls in Yosemite Valley, we consider it to be more broadly applicable to sheeted rock slopes where progressive failures occur. Our analysis also has implications for rock-fall hazard assessment; given the redistribution of stresses that appear to accompany failures along sheeting joints, progressive rock falls might be relatively common in the days to weeks following an initial failure, warranting more detailed investigation and monitoring.

Acknowledgements—We gratefully acknowledge Robert Viesca for the use of a code to calculate stress intensity factors, and Steven Bumgardner for assistance with video analysis. Airborne lidar data were acquired by the National Center for Airborne Laser Mapping (NCALM). We thank William Schulz for an internal USGS review and Florian Amann and Atilla Aydin for journal reviews, all of which served to improve the paper. This research was supported by funding from the Yosemite Conservancy (Stock and Martel), the Landslide Hazards Program of the US Geological Survey (Collins and Harp), the National Science Foundation (Martel, grants EAR05-38334 and CMMI09-19584), and the Jet Propulsion Laboratory (Martel, agreement 1290138).

References

Abellán A, Vilaplana JM, Martinez J. 2006. Application of a long-range terrestrial laser scanner to a detailed rockfall study at Vall de Núria (Eastern Pyrenees, Spain). *Engineering Geology* **88**: 136–148, doi: 10.1016/j.enggeo.2006.09.012.

Atkinson BK. 1984. Subcritical crack growth in geological materials. *Journal of Geophysical Research* **89**: 4077–4114, doi: 10.1029/JB089iB06p04077.

Bahat D, Grossenbacher K, Karasaki K. 1999. Mechanism of exfoliation joint formation in granitic rocks, Yosemite National Park. *Journal of Structural Geology* **21**: 85–96, doi: 10.1016/SO191-814(98)00069-8.

Barber JR. 2002. *Elasticity*, 2nd edn. Kluwer: Dordrecht, The Netherlands.

Bishop AW. 1967. Progressive failure – with special reference to the mechanisms causing it. In *Proceedings of the Geotechnical Conference on Shear Strength Properties of Natural Soils and Rock*, Oslo, Norway, 142–150.

Bjerrum L. 1967. Progressive failure of slopes of over consolidated plastic clays and clay shales. *Journal of the Soil Mechanics Foundations Division of the American Society of Civil Engineers* **93**: 1–49.

Cadman J. 1970. The origin of exfoliation joints in granitic rocks. PhD dissertation, Department of Civil Engineering, University of California, Berkeley.

Chau KT, Shao JF. 2006. Subcritical crack growth of edge and center cracks in façade rock panels subject to periodic surface temperature variations. *International Journal of Solids and Structures* **43**: 807–827, doi: 10.1016/j.ijsolstr.2005.07.010.

Collins BD, Sitar N. 2005. Monitoring of coastal bluff stability using high resolution 3D laser scanning. In *Site Characterization and Modeling, Remote Sensing in Geotechnical Engineering*, Rathje EM (ed.). ASCE Geo-Frontiers Special Publication **138**.

Collins BD, Sitar N. 2008. Processes of coastal bluff erosion in weakly lithified sands, Pacifica, California, USA. *Geomorphology* **97**: 483–501, doi: 10.1016/j.geomorph.2007.09.004.

Cotterell B, Rice JR. 1980. Slightly curved or kinked cracks. *International Journal of Fracture* **16**: 155–169.

Dyskin AV, Germanovich LN, Ustinov KB. 2000. Asymptotic analysis of crack interaction with free boundary. *International Journal of Solids and Structures* **37**: 857–886, doi: 10.1016/S0020-7683(99)00063-3.

Eberhardt E, Stead D, Coggan JS. 2004. Numerical analysis of initiation and progressive failure in natural rock slopes – the 1991 Randa rockslide. *International Journal of Rock Mechanics and Mining Sciences* **41**: 69–87, doi: 10.1016/S1365-1609(03)00076-5.

Einstein H, Veneziano D, Baecher G, O'Reilly K. 1983. The effect of discontinuity persistence on rock slope stability. *International Journal of Rock Mechanics and Mining Sciences* **20**: 227–236.

Erdogan F. 1971. Bonded dissimilar materials containing cracks parallel to the interface. *Engineering Fracture Mechanics* **3**: 231–240, doi: 10.1016/0013-7944(71)90034-8.

Gilbert GK. 1904. Domes and dome structures of the High Sierra. *Bulletin of the Geological Society of America* **15**: 29–36.

Goodman RE, Kieffer DS. 2000. Behavior of rock in slopes. *Journal of Geotechnical and Geoenvironmental Engineering* **126**: 675–684.

Hickman SJ, Svitek J, Borchers J, Scholz E. 1993. In-situ stress measurements at Wawona, Yosemite National Park, California. *Eos Transactions, American Geophysical Union* **74**: 581.

Holister GS. 1967. *Experimental Stress Analysis – Principles and Methods*. Cambridge University Press: Cambridge.

Holzhausen GR. 1989. Origin of sheet structure. 1. Morphology and boundary conditions. *Engineering Geology* **27**: 225–278, doi: 10.1016/0013-7952(89)90035-5.

Huber NK. 1987. The geologic story of Yosemite National Park. *US Geological Survey Bulletin* **1595**.

Ishikawa M, Kurashige Y, Hirakawa K. 2004. Analysis of crack movements observed in an alpine bedrock cliff. *Earth Surface Processes and Landforms* **29**: 883–891, doi: 10.1002/esp.1076.

Jaboyedoff M, Couture R, Locat P. 2009. Structural analysis of Turtle Mountain (Alberta) using digital elevation model: toward a progressive failure. *Geomorphology* **103**: 5–16, doi: 10.1016/j.geomorph.2008.04.012.

Jahns RH. 1943. Sheet structure in granites, its origin and use as a measure of glacial erosion in New England. *Journal of Geology* **51**: 71–98.

Kemeny J. 2005. Time-dependent drift degradation due to the progressive failure of rock bridges along discontinuities. *International Journal of Rock Mechanics and Mining Sciences* **42**: 35–46, doi: 10.1016/j.ijrmms.2004.07.001.

Kemeny J, Kim C. 2009. Increasing our understanding of time-dependent rock mass behavior with ground-based LiDAR, 3D discontinuum modeling, and fracture mechanics. In *Rock Mechanics*, Proceedings of the Second Thailand Symposium, Fuenkojam K, Phien-wej N (eds). Suranaree University of Technology: Thailand, 35–53.

Kim C, Kemeny J. 2009. Progressive failure of a rock slope by the subcritical crack growth of asperities along joints. *Tunnel and Underground Space* **19**: 95–106.

Lawn B. 1993. *Fracture of Brittle Solids*, 2nd ed., Cambridge University Press: Cambridge, U.K.

Maptek. 2011. I-Site Studio three-dimensional LiDAR processing software, Version 3.2, http://www.maptek.com/products/i-site/i-site_studio.html (accessed 25 May 2011).

Martel SJ. 2000. Modeling elastic stresses in long ridges with the displacement discontinuity method. *Pure and Applied Geophysics* **157**: 1039–1057.

Martel SJ. 2006. Effect of topographic curvature on near-surface stresses and application to sheeting joints. *Geophysical Research Letters* **33**: L01308, doi: 10.1029/2005GL024710.

Martel SJ. 2011. Mechanics of curved surfaces, with application to surface-parallel cracks. *Geophysical Research Letters* **38**: L20303, doi: 10.1029/2011GL049354.

Matasci B, Carrea D, Jaboyedoff M, Pedrazzini A, Stock GM, Oppikofer T. 2011. Structural characterization of rockfall sources in Yosemite Valley from remote sensing data and field surveys. *Proceedings of the 2011 Pan-Am Canadian Geological Survey Geotechnical Conference*, Toronto, Ontario, Canada.

Matthes FE. 1930. Geologic history of the Yosemite Valley. US Geological Survey Professional Paper 160.

Muller JR, Martel SJ. 2000. Numerical models of translational landslide rupture surface growth. *Pure and Applied Geophysics* **157**: 1009–1038, doi: 10.1007/s000240050015.

Nara Y, Morimoto K, Yoneta T, Hiroyoshi N, Kaneko K. 2010. Effects of humidity and temperature on subcritical crack growth in sandstone. *International Journal of Solids and Structures* **48**: 1130–1140, doi: 10.1016/j.ijsolstr.2010.12.019.

Nemat-Nasser S, Horii H. 1982. Compression-induced nonplanar crack extension with application to splitting, exfoliation, and rockburst. *Journal of Geophysical Research* **87**: 6805–6821, doi: 10.1029/JB087iB08p06805.

Olson J, Pollard DD. 1989. Inferring paleostresses from natural fracture patterns: A new method. *Geology* **17**: 345–348, doi: 10.1130/0091-7613(1989)017<0345:IPFNFP>2.3.CO;2.

Oppikofer T, Jaboyedoff M, Keusen HR. 2008. Collapse at the eastern Eiger flank in the Swiss Alps. *Nature Geoscience* **1**: 33–37, doi: 10.1038/ngeo258.

Petley DN, Higuchi T, Petley DJ, Bulmer MH, Carey J. 2005. Development of progressive landslide failure in cohesive materials. *Geology* **33**: 201–204, doi: 10.1130/G21147.1.

Pollard DD, Holzhausen G. 1979. On the mechanical interaction between a fluid-filled fracture and the earth's surface. *Tectonophysics* **53**: 27–57, doi: 10.1016/0040-1951(79)90353-6.

Pollard DD, Aydin A. 1984. Propagation and linkage of oceanic ridge segments. *Journal of Geophysical Research* **89**: 10,017–10,028, doi: 10.1029/JB089iB12p10017.

Pollard DD, Segall P. 1987. Theoretical displacements and stresses near fractures in rocks: with applications to faults, joints, veins, dikes, and solution surfaces. In *Fracture Mechanics of Rock*, Atkinson BK (ed). Academic: San Diego; 277–349.

Rabatel A, Deline P, Jaillet S, Ravanel L. 2008. Rock falls in high-alpine rock walls quantified by terrestrial LiDAR measurements: a case study in the Mont Blanc area. *Geophysical Research Letters* **35**: L10502, doi: 10.1029/2008GL033424.

Rosser NJ, Dunning SA, Lim M, Petley DN. 2005. Terrestrial laser scanning for quantitative rockfall hazard assessment. In *Landslide Risk Management*, Hungr O, Fell R, Couture R, Eberhardt E (eds). Balkema: Amsterdam.

Rosser NJ, Lim M, Petley DN, Dunning SA, Allison RJ. 2007. Patterns of precursory rockfall prior to slope failure. *Journal of Geophysical Research: Earth Surface* **112**: F04014, doi: 10.1029/2006JF000642.

Sanderson F, Bakkehoi S, Hestnes E, Lied K. 1996. The influence of meteorological factors on the initiation of debris flows, rockfalls, rockslides, and rockmass stability. In *Landslides*, Senneset K (ed). Balkema: Rotterdam.

Stein RS, Barka AA, Dieterich JH. 1997. Progressive failure on the North Anatolian fault since 1939 by earthquake stress triggering. *Geophysical Journal International* **128**: 594–604, doi: 10.1111/j.1365-246X.1997.tb05321.x.

Stock GM, Bawden GW, Green JK, Hanson E, Downing G, Collins BD, Bond S, Leslar M. 2011. High-resolution three-dimensional imaging and analysis of rock falls in Yosemite Valley, California. *Geosphere* **7**: 573–581, doi: 10.1130/GES00617.1

Terzaghi K. 1950. Mechanism of landslides. In *Application of Geology to Engineering Practice*. Geological Society of America Special Publication, Berkey Volume; 83–123.

Terzaghi K. 1962. Stability of steep slopes on hard unweathered rock. *Geotechnique* **12**: 251–263.

Timoshenko SP, Goodier JN. 1970. *Theory of Elasticity*. McGraw-Hill: New York.

Vargas Jr EA, Chavez E, Gusmão L, Amaral C. 2009. Is thermal fatigue a possible mechanism for failures of some rock slopes in Rio de Janeiro, Brazil? American Rock Mechanics Association, 43rd US Rock Mechanics Symposium, Asheville, North Carolina, 09–126.

Wieczorek GF, Jäger S. 1996. Triggering mechanisms and depositional rates of postglacial slope movement processes in the Yosemite Valley, California. *Geomorphology* **5**: 17–31, doi: 10.1016/0169-555X(95)0012-I.

Wieczorek GF, Snyder JB. 1999. Rock falls from Glacier Point above Camp Curry, Yosemite National Park, California. U. S. Geological Survey Open-File Report 99–385, http://pubs.usgs.gov/of/1999/ofr-99-0385/pdf.

Wieczorek GF, Snyder JB. 2004. Historical rock falls in Yosemite National Park, California. U.S. Geological Survey Open-File Report 03–491, http://pubs.usgs.gov/of/2003/ofr-03-491.pdf.

Wieczorek GF, Stock GM, Reichenbach P, Snyder JB, Borchers JW, Godt JW. 2008. Investigation and hazard assessment of the 2003 and 2007 Staircase Falls rock falls, Yosemite National Park, California, USA. *Natural Hazards and Earth System Sciences* **8**: 421–432, www.nat-hazards-earth-syst-sci.net/8/421/2008/.

Zimmer V, Collins BD, Stock GM, Sitar N. 2012. Rock fall dynamics and deposition: An integrated analysis of the 2009 Ahwiyah Point rock fall, Yosemite National Park, USA. *Earth Surface Processes and Landforms* (in press).